Mapping the Floor of Yellowstone Lake: New Discoveries from High-Resolution Sonar Imaging, Seismic-Reflection Profiling, and Submersible Studies

L. A. Morgan, W. C. Shanks III, D. Lovalvo, M. Webring, G. Lee, W. J. Stephenson, and S. Y. Johnson

"…we arrived at the summit of the first ridge…It was a pretty steep climb to the top of it, over a volcanic sand composed of broken down obsidian which composed the only rocks around us."
—Albert Peale, mineralogist,
U.S. Geological Survey, Hayden Survey, August 6, 1871.

Abstract

Recently completed multi-beam sonar-imaging and seismic-reflection surveys of the northern, West Thumb, and central basins of Yellowstone Lake provide insight into post-caldera volcanism and active hydrothermal processes occurring in a large lake environment above a cooling magma chamber. High-resolution mapping of the lake floor reveals an irregular lake bottom covered with dozens of features directly related to hydrothermal, tectonic, volcanic, and sedimentary processes. Newly mapped rhyolitic lava flows that underlie much of Yellowstone Lake exert fundamental control on lake geology, basin bathymetry, and localization of hydrothermal vent sites. Imaged and identified features include over 150 hydrothermal vent sites, several very large (>500 m diameter) and many small hydrothermal explosion craters (~1-200 m diameter), elongate fissures cutting post-glacial (<12 ka) sediments, siliceous hydrothermal spires as tall as 8 m, sublacustrine landslide deposits, deformed lacustrine sediments associated with domal structures and hydrothermal vents, submerged former shorelines, and a recently active graben, all occurring within the southeast margin of the 0.640-Ma Yellowstone caldera. Sampling and observations with a submersible remotely operated vehicle (ROV) confirm and extend our understanding of many of the identified features.

Introduction

Several powerful geologic processes in Yellowstone National Park have contributed to the unusual shape of Yellowstone Lake, which straddles the southeast margin of the Yellowstone caldera (Figure 1). Volcanic forces contributing to the lake's form include the 2.057 ± 0.005-Ma (1-σ) caldera-forming eruption of the Huckleberry Ridge Tuff followed by eruption of the 0.640 ± 0.002-Ma Lava Creek Tuff to form the Yellowstone caldera (Christiansen 1984; Christiansen 2001; Hildreth et al. 1984; U.S.G.S. 1972). A smaller caldera-forming event

about 140 ka, comparable in size to Crater Lake, Oregon, created the West Thumb basin (Christiansen 1984; Christiansen 2001; Hildreth et al. 1984; U.S.G.S. 1972). Large-volume postcaldera rhyolitic lava flows are exposed west of the lake (Figure 1B). Several significant glacial advances and recessions overlapped the volcanic events (Pierce 1974; Pierce 1979; Richmond 1976; Richmond 1977) and helped to deepen the fault-bounded South and Southeast Arms (Figure 1B). More recent dynamic processes shaping Yellowstone Lake include currently active fault systems, erosion of a series of postglacial shoreline terraces, and postglacial (<12 ka) hydrothermal-explosion events, which created the Mary Bay crater complex and other craters.

Formation of hydrothermal features in Yellowstone Lake is related to convective meteoric hydrothermal fluid circulation above a cooling magma chamber. Hydrothermal explosions result from accumulation and release of steam generation during fluid ascent, possibly reflecting changes in confining pressure that accompany and may accelerate failure and fragmentation of overlying cap rock. Sealing of surficial discharge conduits due to hydrothermal mineral precipitation also contributes to over-pressuring and catastrophic failure. Heat-flow maps show that both the northern and West Thumb basins of Yellowstone Lake have extremely high heat flux compared to other areas in the lake (Morgan et al. 1977). Earthquake epicenter locations indicate that the area north of the lake is seismically active (Smith 1991), and ROV studies identify hydrothermally active areas within the lake (Klump et al. 1988; Remsen et al. 1990).

Objectives of this work include understanding the geologic processes that shape the lake and how they affect the present-day lake ecosystem. Our three-pronged approach to mapping the floor of Yellowstone Lake is designed to locate, image, and sample bottom features such as sublacustrine hot-spring vents and fluids, hydrothermal deposits, hydrothermal-explosion craters, rock outcrops, slump blocks, faults, fissures, and submerged shorelines. Chemical studies of the vents indicate that 20 percent of the total deep thermal water flux in Yellowstone National Park occurs on the lake bottom (Morgan et al. 2003). Hydrothermal fluids containing potentially toxic elements (As, Sb, Hg, Mo, W, and Tl) significantly affect lake chemistry and possibly the lake ecosystem. ROV observations indicate that shallow hydrothermal vents are home to abundant bacteria and amphipods that form the base of the food chain, which includes indigenous cutthroat trout, piscivorous exotic lake trout, and grizzly bears, bald eagles, and otters that feed on the potamodromous cutthroat trout during spawning in streams around the lake. Finally, our results document and identify potential geologic hazards associated with sublacustrine hydrothermal explosions, landslides, faults, and fissures in America's premier National Park.

Methods

Yellowstone Lake mapping and sampling conducted in 1999 through 2001 as a collaborative effort between the U.S. Geological Survey, Eastern Oceanics, and the National Park Service (Yellowstone National Park) utilized bathymetric, seismic, and submersible remotely operated vehicle (ROV) equipment as follows.

Figure 1A.

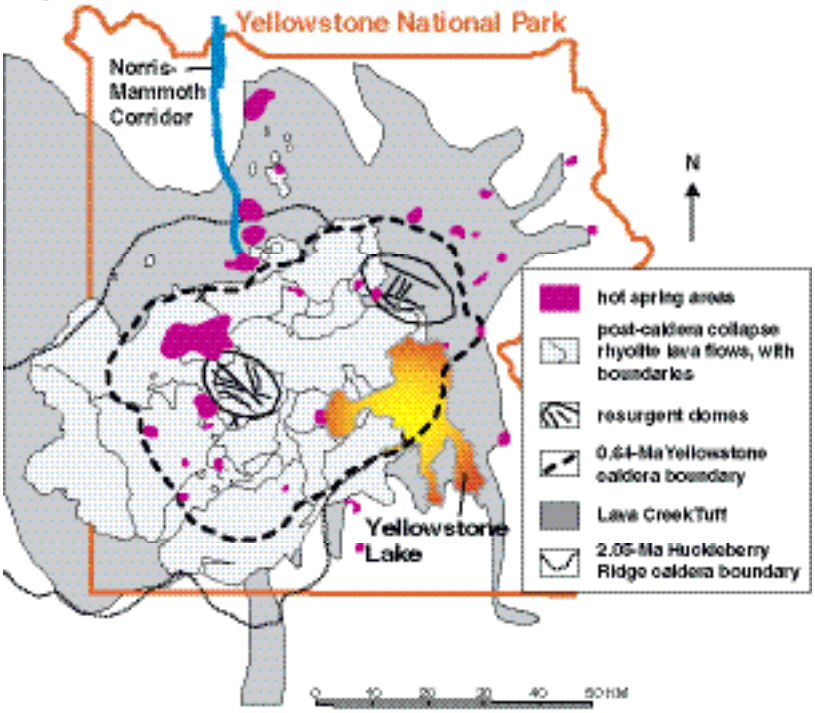

Figure 1B.

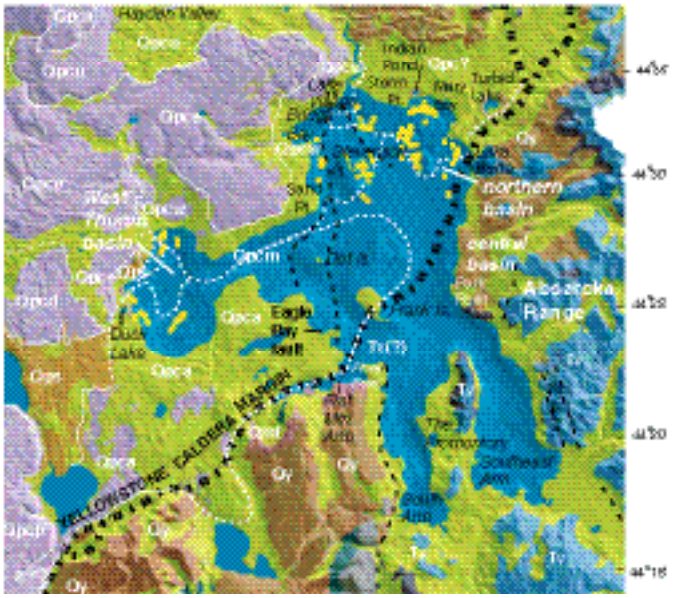

Figure 1. (A) Index map showing the 0.640-Ma Yellowstone caldera, the distribution of its erupted ignimbrite (the Lava Creek Tuff, medium gray), post-caldera rhyolitic lava flows (light gray), subaerial hydrothermal areas (red), and the two resurgent domes (shown as ovals with faults). The inferred margin of the 2.05-Ma Huckleberry Ridge caldera is also shown. Data are from Christiansen 2001. (B) Geologic shaded relief map of the area surrounding Yellowstone Lake in Yellowstone National Park. Geologic mapping is from USGS 1972 and Yellowstone Lake bathymetry is from Kaplinski 1991. Yellow markers in West Thumb basin and the northern basin are locations of active or inactive hydrothermal vents mapped by seismic reflection and multibeam sonar. The lithologic symbols are as follows: Tv = Tertiary volcanic rocks; Qps = tuff of Bluff Point; Qpcd = Dry Creek flow; Qpcm = Mary Lake flow; Qpca = Aster Creek flow; Qpcw = West Thumb flow; Qpce = Elephant Back flow; Qpch = Hayden Valley flow; Qpcn = Nez Perce flow; Qpcp = Pitchstone Plateau flow; Qs = Quaternary sediments (yellow); Qy = Quaternary Yellowstone Group ignimbrites (brown; Christiansen 2001; USGS 1972). Location of Yellowstone caldera margin is from Christiansen 1984, with slight modifications from Finn and Morgan 2002. Funding for the color images printed in this article was provided by the U.S.G.S.

Multi-beam swath-bathymetric surveys were conducted using a SeaBeam 1180 (180 kHz) instrument with a depth resolution of about 1% water depth. Water depth varied from ~4 to 133 m in the survey areas. The multi-beam instrument uses 126 beams arrayed over a 150° ensonification angle to map a swath width of 7.4 times water depth. In the West Thumb basin survey, 99% complete bathymetric coverage was accomplished using the multi-beam system whereas the northern Yellowstone Lake coverage was 95%. Sub-bottom seismic reflection profiling was done with an EdgeTech SB-216S, which sweeps a frequency range from 2 to 16 kHz and has a beam angle of 15–20°. Both the swath unit transducer and the sub-bottom unit were rigidly mounted to the transom of an 8-m aluminum boat used for survey purposes. The Eastern Oceanics submersible ROV is a small vehicle (~1.5 m x 1 m x 1 m) attached to the vessel with a 200-m tether that provides live videographic coverage and remote control of submersible thrusters, cameras, and sampling equipment. This vehicle has a full-depth rating of 300 m and is capable of measuring temperature, conductivity, and depth and of retrieving uncontaminated hydrothermal vent water samples and rock samples up to ~40 cm-long. Previous bathymetric mapping of the lake used a single-channel echo sounder and a mini-ranger for navigation (Kaplinski 1991) requiring interpolation between lines. The new swath multi-beam survey produced continuous overlapping coverage, producing high-resolution bathymetric images and seismic records of the upper 25 m of the lake bottom.

Flow modeling was carried out using the program Basin2, v. 4.0.1, 1982–1999, developed by Craig Bethke, University of Illinois. This program uses finite difference methods to solve Darcy's law for fluids of varying density. The program allows the user to model topographic, compaction-driven, and/or convective flow by setting parameters related to fluid density, heat capacity, heat flow, porosity and permeability. Lava flow schematic shown in Figure 4 modified from (Bonnichsen and Kauffman 1987).

Interpretation of Individual Features

Margin of the caldera: Mapping of Yellowstone Lake has been primarily in the 0.64-Ma Yellowstone caldera but it was not until the central basin was mapped that the margin of the caldera was identified, here as a series of elongate troughs. Geologic maps show the margin of the Yellowstone caldera entering the western part of Yellowstone Lake at the entrance to Flat Mountain Arm and resurfacing north of Lake Butte (Figure 1B). The location of the caldera margin between these points has had various interpretations, based primarily on lower resolution bathymetry. Previous interpretations include a margin trending north of Frank Island as well as an inferred margin south of Frank Island. Based on new data, we infer the margin of the Yellowstone caldera to pass through the southern part of Frank Island.

High-resolution aeromagnetic maps (Finn and Morgan 2002) of Yellowstone Lake show a series of discontinuous moderate amplitude negative magnetic anomalies in the southeast part of the central basin (Figure 2A). These anomalies coincide with bathymetric lows as identified in the new sonar image mapping. Careful examination of the bathymetry on Figure 3 shows these lows to extend as a series of elongated troughs northeast from Frank Island across the deep basin of the lake. Similar, though somewhat smaller, troughs emerge on the western side of Frank Island and continue toward the head of Flat Mountain Arm. Here, the caldera margin separates Tertiary andesitic rocks and pre-caldera and caldera rhyolitic rocks to the south from young, post-caldera rhyolites to the north and northwest.

Examination of the reduced-to-the-pole aeromagnetic map shows pronounced positive magnetic anomalies over the Absaroka Range along the eastern side of Yellowstone Lake (Figure 2A). Rugged topographic relief and predominantly highly magnetized rock give the area its high positive magnetic character. Similarly magnetized material occurs along Promontory Point where Tertiary andesitic lava and debris flows are prominently exposed in cliffs several hundred meters thick. The magnetic signature is repeated north and east of Plover Point in southern Yellowstone Lake and along the eastern shore of the lake near the outlet for Columbine Creek. Finn and Morgan (2002) suggest that this series of positive magnetic anomalies are caused by Tertiary volcanic rocks at the surface, as exposed at Promontory Point and in the Absaroka Range, or buried at shallow depths in the lake, such as north of Plover Point northward into the southern third of Frank Island or due west along the eastern shore (Figure 2A).

From west to east, we interpret the margin of the caldera within the lake to pass in a general eastern direction following Flat Mountain Arm, then northeastward cutting through the southern part of Frank Island, and then again northeastward (Figure 3). The amplitudes of magnetic anomalies on the northern part of Frank Island are similar in character as those associated with postcaldera rhyolitic lava flows, such as much of the West Thumb, Hayden Valley, or Aster Creek flows (Figure 2A). In contrast, the amplitude of the magnetic anomaly on the southern side of the island is steeper of greater magnitude and similar to that seen in the Absaroka or Promontory Point. This location of the caldera margin

based on mapped geology on land and the series of magnetic anomalies in the lake is consistent with the recently acquired bathymetry (Figures 1, 2, 3).

Rhyolitic lava flows: A major discovery of the surveys is the presence of previously unrecognized rhyolitic lava flows on the floor of the lake. The lava flows are key to the control of many geologic and hydrologic features in the lake.

Areas of the lake bottom around the perimeter of West Thumb basin (Figure 3) have steep, nearly vertical margins, bulbous edges, and irregular hummocky surfaces. Seismic-reflection profiles in the nearshore areas of West Thumb basin show high-amplitude reflectors beneath about 7–10 m of layered lacustrine sediments (Figure 4A). We interpret these sublacustrine features to be buried rhyolitic lava flows that partly fill the interior of the 140-ka West Thumb caldera. Subsequent sampling with the submersible ROV collected rhyolite from an inferred lava-flow area in east-central West Thumb basin.

In the northern and central basins, similar features also are present. Sublacustrine rhyolitic lava flows in the northern and northeastern areas of the northern basin are inferred from the bathymetry and do not have mapped subaerial equivalents. These features also could represent shallow rhyolitic intrusions. A dominant lithic clast present in the hydrothermal explosion breccia of Mary Bay and prevalent in the alluvium of the lower Pelican Valley (Figure 1B) is a quartz-rich porphyry that has not been described before. These porphyry clasts may be derived from a buried volcanic unit in the lower Pelican Valley that may be producing the moderate positive magnetic anomaly seen here (Finn and Morgan 2002) (Figure 2).

Large-volume rhyolitic lava flows (10's of km^3) on the Yellowstone Plateau control much of the local hydrology. Stream drainages tend to occur along flow boundaries, rather than within flow interiors. Characteristic lava-flow morphologies include near-vertical margins (some as high as 700 m), rubbly flow carapaces, hummocky or ridged tops, and strongly jointed interiors. Spherulitic and lithophysal zones commonly include large cavities. Many flows have vitrophyric exterior rinds with shrinkage cracks and sheet-jointed crystallized interior zones. Breccias occur locally.

In many exposures of postcaldera rhyolite lava flows near the current margins of Yellowstone Lake, including West Thumb basin, and north of the lake in Hayden Valley, ample evidence exists for interaction between emplacement of hot rhyolitic lava flows and standing water. Clastic dikes, highly fractured perlitic vitrophyre, massive rhyolitic breccias with fine-grained and altered matrix, and entrained stream, beach, and lake sediments point to emplacement of lavas in an aqueous environment.

Magnetic signature of rhyolitic lava flows: Comparison of the new high-resolution aeromagnetic maps (Finn and Morgan, 2002) (Figure 2) with geologic maps (Figure 1B) (Blank 1974; Christiansen 1974; Christiansen and Blank 1975; Richmond 1973) shows a close relationship of magnetic anomalies to the mapped individual lava flows. Moderate-amplitude positive magnetic anomalies coincide with the mapped extent of subaerial post-caldera rhyolitic lava flows (Finn and Morgan 2002) and extend into the sublacustrine environment in many

Figure 2A.

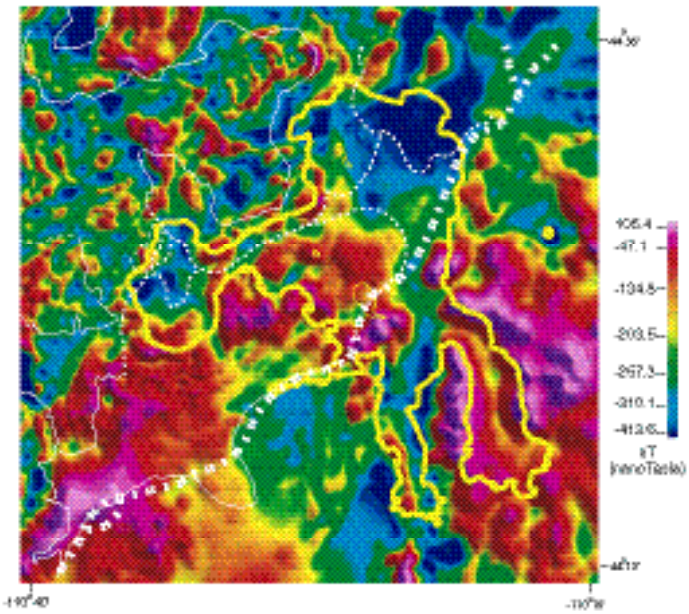

Figure 2B.

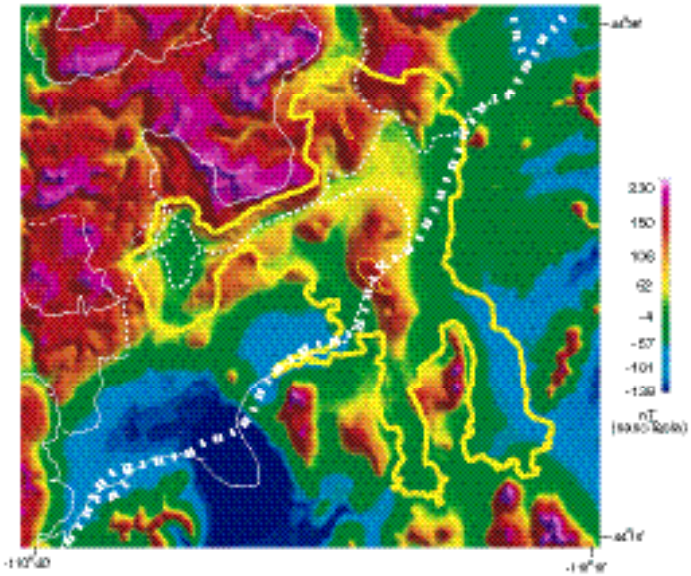

Figure 2. (A) Color shaded-relief image of high-resolution, reduced-to-the-pole aeromagnetic map (Finn and Morgan 2002). Sources of the magnetic anomalies are shallow and include the post-caldera rhyolite lava flows (some outlined in white), which have partly filled in the Yellowstone caldera. Commonly, rhyolitic lava-flow margins have impermeable glassy rinds that are not subject to hydrothermal alteration, producing distinctive positive magnetic anomalies. Extensive areas of negative magnetic anomalies in the West Thumb and northern basins and along the caldera margin northeast of the lake are areas of high heat flow and intense present and past hydrothermal alteration, as suggested by sublacustrine vent locations (Figure 1B). (B) Color-shaded relief image of the magnetic anomaly due to uniformly magnetized terrain in the present Earth's field direction of inclination =70˚ and a declination of 15˚ with an intensity of 2.5 A/m, and then reduced to the pole (Finn and Morgan 2002). Rhyolitic lava flows (outlined in white) underlying Yellowstone Lake are shown clearly on this map.

areas (Figures 1, 2, 3). For example, northwest of the northern lake basin, moderate-amplitude magnetic anomalies correspond to mapped subaerial postcaldera rhyolitic lava flows (Figure 1B) and extend from land into the lake (Figure 2A). Similarly, mapped subaerial lava flows around West Thumb basin and west of the central lake basin can be extended into the lake based on moderate amplitude positive magnetic anomaly patterns (Figure 2). These characteristic magnetic signatures, in combination with the new bathymetric and seismic data, allow identification and correlation of rhyolitic lava flows well out into the lake.

In the northern basin, negative magnetic anomalies (Figure 2A) are extensive. Excessively high heat flow in the Mary Bay area (1,550–15,600 mW/m^2) (Morgan et al. 1977), in part related to proximity to the margin of the Yellowstone caldera, indicates that hydrothermal activity has destroyed or significantly reduced the magnetic susceptibility of minerals in rocks and sediments producing the observed negative magnetic anomalies. Comparison of the reduced-to-the-pole magnetic anomalies (Figure 2A) with those caused by uniformly magnetized terrain (Figure 2B) draws attention to areas, such as in the northern basin at Mary Bay or near Stevenson Island, with buried magnetic sources or places where the surficial lava flows are not as magnetic or are thinner than expected. While the shape of the observed magnetic anomaly mimics that caused by terrain, the amplitudes of the anomalies are different, possibly implying that topography contributes to the observed anomaly but has a magnetization different than calculated. In this case, we interpret the topography as representing large, unidentified rhyolitic lava flows.

Variations in total field magnetic intensity and susceptibility (Finn and Morgan 2002) appear to correspond, in part, to the degree of alteration present in the rhyolite that produces the anomaly. In many exposures where a flow is glassy, flow-banded, and fresh, such as the West Thumb rhyolite flow due west of the Yellowstone River (Figures 2A, 3), the magnetic anomaly of the exposure generally appears as positive. In contrast, in many exposures where evidence for emplacement of the flow into water or ice is present, such as the West Thumb rhyolite flow exposed on the northeast shore of West Thumb basin (Figures 2A, 3), the magnetic anomaly is negative (Figure 2A). All of the postcaldera rhyolites have a normal magnetic remanence, being emplaced during the past 160 ka

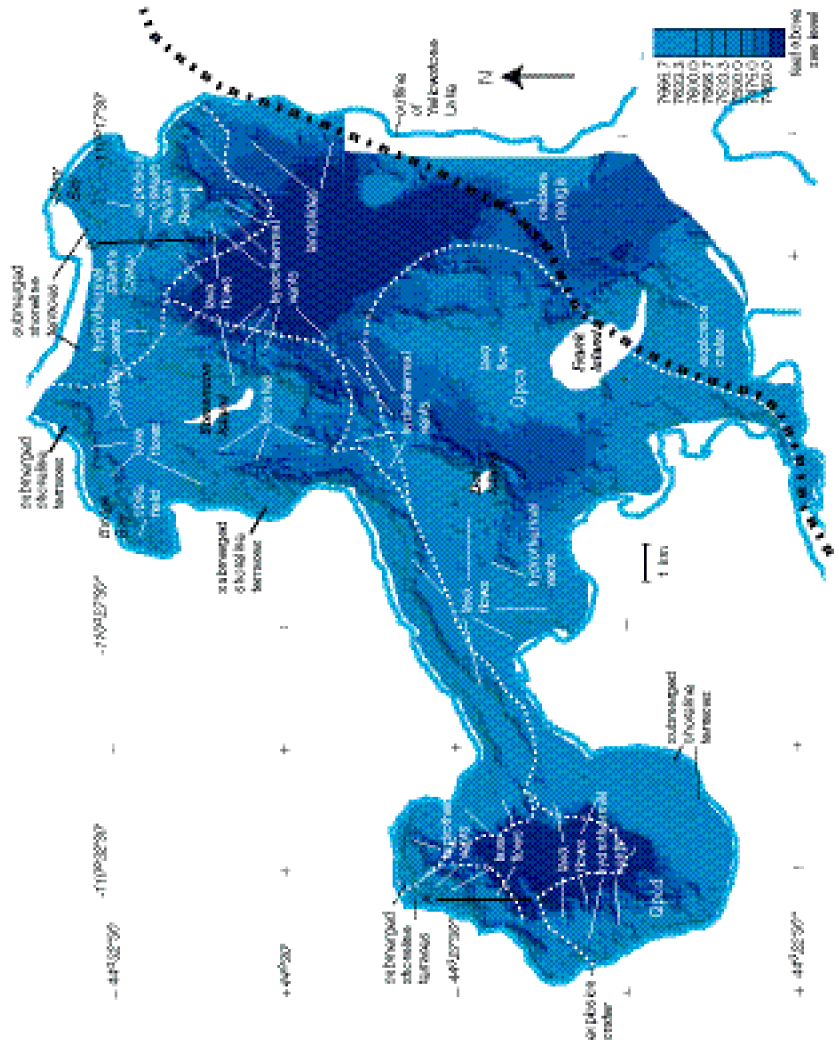

Figure 3.

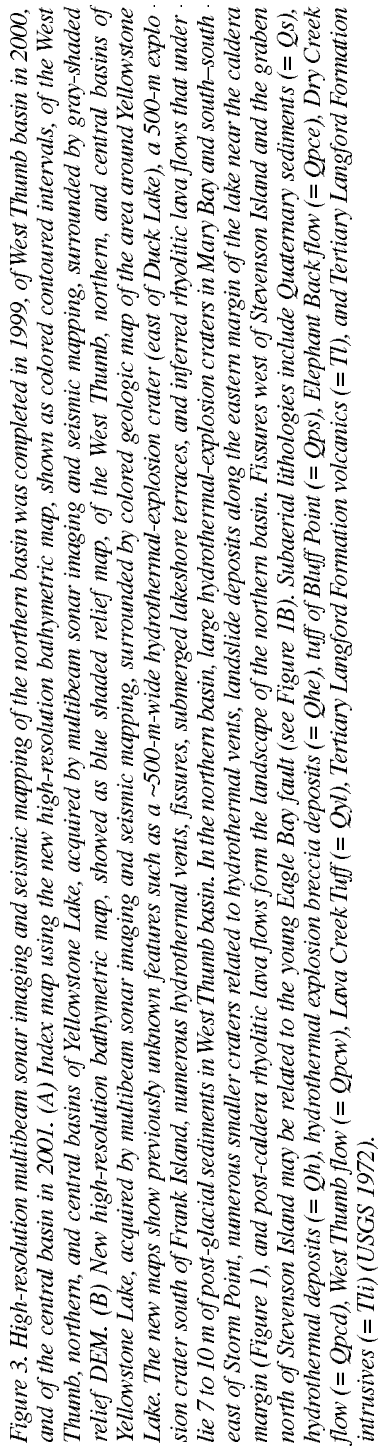

Figure 3. High-resolution multibeam sonar imaging and seismic mapping of the northern basin was completed in 1999, of West Thumb basin in 2000, and of the central basin in 2001. (A) Index map using the new high-resolution bathymetric map, shown as colored contoured intervals, of the West Thumb, northern, and central basins of Yellowstone Lake, acquired by multibeam sonar imaging and seismic mapping, surrounded by gray-shaded relief DEM. (B) New high-resolution bathymetric map, showed as blue shaded relief map, of the West Thumb, northern, and central basins of Yellowstone Lake, acquired by multibeam sonar imaging and seismic mapping, surrounded by colored geologic map of the area around Yellowstone Lake. The new maps show previously unknown features such as a ~500-m-wide hydrothermal-explosion crater (east of Duck Lake), a 500-m explosion crater south of Frank Island, numerous hydrothermal vents, fissures, submerged lakeshore terraces, and inferred rhyolitic lava flows that underlie 7 to 10 m of post-glacial sediments in West Thumb basin. In the northern basin, large hydrothermal-explosion craters in Mary Bay and south–south-east of Storm Point, numerous smaller craters related to hydrothermal vents, landslide deposits along the eastern margin of the lake near the caldera margin (Figure 1), and post-caldera rhyolitic lava flows form the landscape of the northern basin. Fissures west of Stevenson Island and the graben north of Stevenson Island may be related to the young Eagle Bay fault (see Figure 1B). Subaerial lithologies include Quaternary sediments (= Qs), hydrothermal deposits (= Qh), hydrothermal explosion breccia deposits (= Qhe), tuff of Bluff Point (= Qps), Elephant Back flow (= Qpce), Dry Creek flow (= Qpcd), West Thumb flow (= Qpcw), Lava Creek Tuff (= Qyl), Tertiary Langford Formation volcanics (= Tl), and Tertiary Langford Formation intrusives (= Tli) (USGS 1972).

(Christiansen 2001); thus, susceptibility is the primary variable and ranges from 10^{-3} for relatively pristine rocks to 10^{-6} for extensively hydrothermally altered rocks (Finn and Morgan 2002).

Rhyolitic lava flows control geothermal activity: The floor of Yellowstone Lake, two-thirds of which is within the Yellowstone caldera, lies above a large cooling magma chamber (Eaton et al. 1975; Fournier 1989; Fournier et al. 1976; Lehman et al. 1982; Stanley et al. 1991; Wicks et al. 1998). The new high-resolution bathymetry of the northern, central, and West Thumb basins of Yellowstone Lake shows that many hydrothermal features in the surveyed areas are located within or along edges of areas of high relief, interpreted as rhyolitic lava flows (Figures 1B, 3). Based on our observations of the abundant present-day distribution of hydrothermal vents (Figures 1B, 3), we infer that the rhyolitic lava flows act as a cap rock exerting influence on the flow of thermal water. Upwelling hydrothermal fluids are focused preferentially through the basal breccia deposits and fractures of the rhyolitic lava flows whereas hydrothermal fluids conducted through lake and glacial sediments tend to be more diffuse (Figure 5A).

In order to evaluate the effect of rhyolitic lava flows on convective fluid flow in the sublacustrine environment, a pair of simple two-dimensional flow models was constructed (Figure 5B, C). The first model involves fluid flow in a sediment volume 1-km thick by 10-km wide (Figure 5B) covered by lake water 200 m deep. Both left and right edges of the sediment volume are open to flow. Vertical-direction (z) permeability is 0.001 darcy and horizontal-direction (x) permeability is 0.01 darcy, properties expected for lacustrine or glacial sediments. In order to simulate a magma chamber at depth, heat flow through the base of

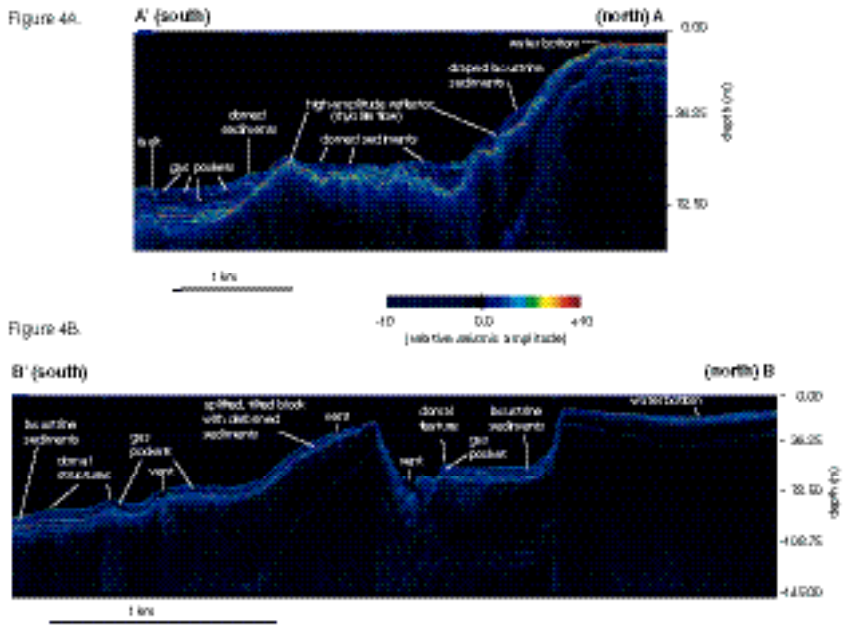

Figure 4. (A) High-resolution seismic-reflection image from northwestern West Thumb basin showing high-amplitude (red) reflector interpreted as a sub-bottom rhyolitic lava flow. Glacial and lacustrine sediments, marked in blue, overlie this unit. The data amplitudes have been debiased and spatially equalized only. No additional gain corrections or filtering are applied. (B) High-resolution seismic-reflection image (line YL72) across part of Elliott's explosion crater, showing small vents, gas pockets, and domed sediments in the lacustrine sediments that overlie the crater flank. Lacustrine sediment thickness in the main crater indicates 5,000–7,000 years of deposition since the main explosion. More recent explosions in the southern part of the large crater ejected post-crater lacustrine sediments and created new, smaller craters and a possible hydrothermal siliceous spire. Lava flow schematic modified from Bonnichsen and Kauffman 1987.

the section is set at 4 HFU or about 167.6 mW/m^2 (1 heat flow unit = 10^{-6} cal/cm^2/sec = 41.9 mW/m^2), much higher than a typical continental value of 40–70 mW/m^2. Results indicate uniform increase of temperature with depth, recharge at the surface, flow out both ends, and flow rates of <1 mm/yr. The basal heat flow value used in these calculations produces the highest possible thermal gradient without violating the assumptions of the modeling approach (boiling not allowed, fluid density and viscosity extremes not allowed, fluid temperature <300°C).

Addition of a sublacustrine 200-m-thick cap rock, in this case a fully cooled lava flow, on top of the model sedimentary section (Figure 5C) produces dramatic changes in fluid flow. The lava flow is assigned permeabilities of 0.02 darcy in the z-direction and 0.045 darcy in the x-direction, within the range measured for fractured volcanic rocks. Results indicate that a thick cap rock, in

this case a sublacustrine lava flow, atop the sediment causes localization of intense thermal upflow through the lava flow and strong discharge at the surface of the flow. Fluid flow rates in the model range up to 160 mm/yr and temperatures to >130°C. In the natural situation, localization of upflow is expected along fracture zones, producing focused hydrothermal vents. Field observations and this physical model may explain the preferential distribution of hydrothermal vents and explosion craters located within or at the edges of rhyolitic lava flows in Yellowstone Lake.

Large hydrothermal explosion craters: Large (>500 m) circular, steep-walled, flat-bottomed depressions are mapped at several sites in the West Thumb, central, and northern lake basins (Figures 3, 5) and are interpreted as large composite hydrothermal explosion craters. A newly discovered 500-m-wide sublacustrine explosion crater in the western part of West Thumb basin near the currently active West Thumb geyser basin is only 300 m east of Duck Lake (Figure 3), a postglacial (<12 ka) hydrothermal explosion crater (Christiansen 1974; Christiansen 2001; Richmond 1973; U.S.G.S. 1972). Here, heat-flow values are as high as 1500mW/m^2 (Morgan et al. 1977) and reflect the hydrothermal discharge that contributed to the formation of this explosion crater. The 500-m-wide West Thumb explosion crater is surrounded by 12- to 20-m high nearly vertical walls and has several smaller nested craters along its eastern edge. These nested craters are as deep as 40 m and have more conical forms reflecting their younger ages relative to the main crater. Temperatures of hydrothermal fluids emanating from the smaller northeast nested crater have been measured at 72°C by ROV.

In the northern basin of Yellowstone Lake, Mary Bay represents a roughly 1-km by 2-km area of coalesced explosion craters (Morgan et al. 1998; Wold et al. 1977) (Figure 3) in an area of extremely high heat flow (Morgan et al. 1977). Radiocarbon dates from charcoal in and carbonized soils below the ejected breccia deposit exposed in the wave-cut cliffs along the shore of Mary Bay indicate that eruption of this crater occurred at 10.8 ka (Morgan et al. 1998). Detailed stratigraphic measurements of the breccia deposit indicate that multiple explosions and emplacements occurred during formation of this large and complex feature. Submersible investigations show that hydrothermal vent fluids from a 35-m-deep crater in the Mary Bay complex have temperatures near the 120°C limit of the temperature probes.

One kilometer southwest of the Mary Bay crater complex is another large (~800 m diameter) composite depression we informally refer to as Elliott's Crater (Figure 6), named after Henry Elliott who helped map Yellowstone Lake in the Hayden survey (Merrill 1999) in 1871. Development of Elliott's explosion crater is best illustrated in a north-south seismic reflection profile (Figure 4B). Zones of non-reflectivity in the seismic profile on the floor and flanks of the large crater are probably hydrothermally altered and possibly heterolithologic explosion-breccia deposits, similar in character to those exposed on land and associated with subaerial explosion craters. Seismic profiles of the hummocky area southeast of Elliott's crater also are non-reflective and may represent a layer of

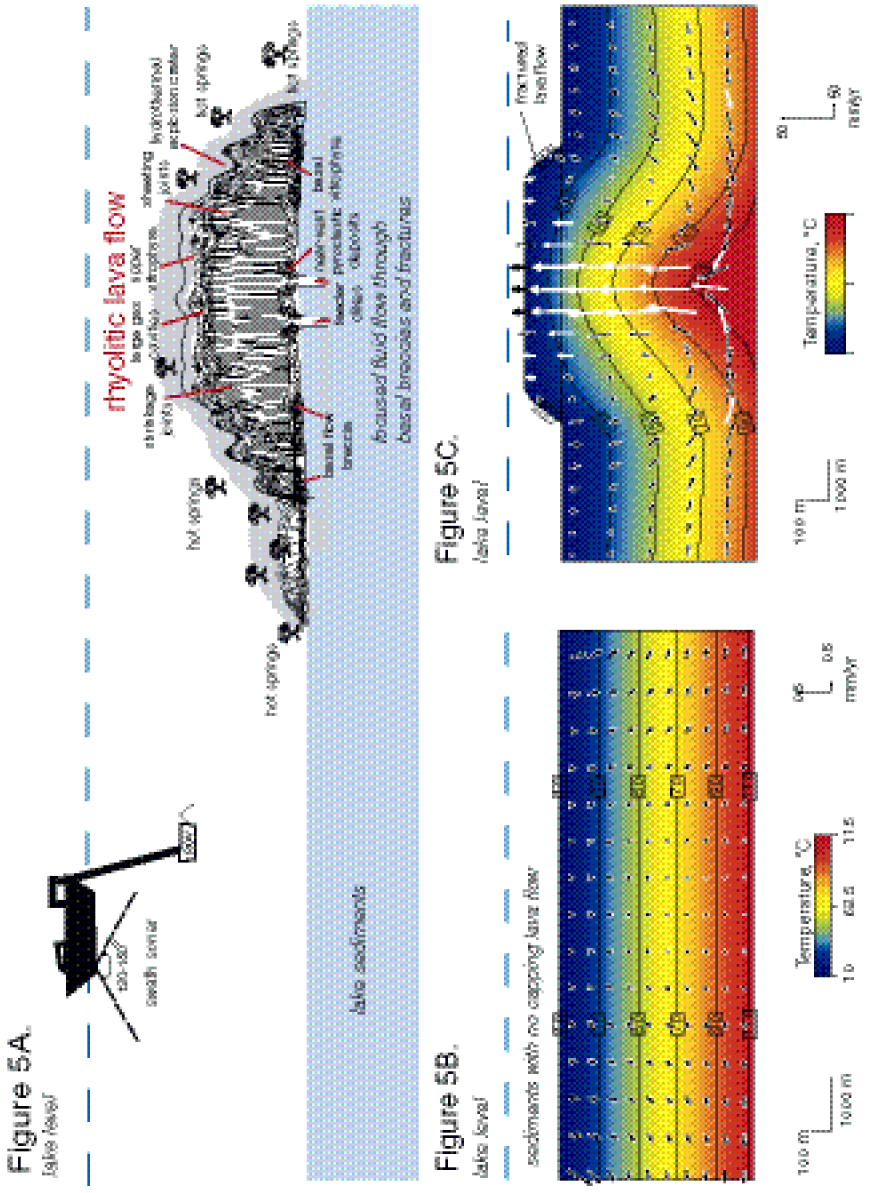
Figure 5A.
lake level
120–180°
swath sonar
rhyolitic lava flow
hot springs
lake sediments
fractured fluid flow through
basal breccias and fractures
Figure 5B.
lake level
sediments with no capping lava flow
100 m
1000 m
Temperature, °C
10
115
0.5
mm/yr
Figure 5C.
lake level
fractured
lava flow
100 m
1000 m
Temperature, °C
50
mm/yr

Figure 5. (A) Schematic diagram showing physical features of a rhyolitic lava flow (modified from Bonnichsen and Kauffman 1987). (B) Fluid-flow model with simple sandstone aquifer (no caprock), which results in low flow velocities, recharge at the surface, and lateral flow out of both ends of the model aquifer. Even though heat flow is the same as in (C), subsurface temperatures in this model never exceed 110°C and strong convection cells are not established. (C) Fluid-flow model with a fully cooled rhyolitic lava flow acting as caprock. The underlying sandstone aquifer and heat flow are exactly the same as in (B). The addition of a 200-m-thick fractured crystalline rock cap strongly focuses the upward limb of an intense convection cell under the caprock. In this model, fluid temperatures reach 130°C, and flow velocities are 100 times higher than in the uncapped aquifer (B).

heterolithic and/or hydrothermally altered material erupted from this crater.

Following the initial major explosive event, lacustrine sediments, imaged as laminated reflective layers in the seismic profile (Figure 4B), accumulated in the floor of the crater and on its south flank. Opaque zones within the stratified sedimentary fill of the crater indicate the presence of gas. The presence of two V-shaped vents at the south end of the crater floor further indicates recent hydrothermal activity within the explosion crater. Two additional hydrothermal vents imaged in Figure 4B occur on the south flank, outside of the crater. These vent areas differ slightly in morphology from the nested vents within Elliott's Crater. These flank vents may have formed by collapse resulting from vigorous hydrothermal activity, extensive hydrothermal alteration, and structural failure of the overlying cap rock.

The seismic profile shows about 80 m of vertical relief between the current lakeshore and the average depth of the deeper lake basin several km south of Mary Bay (Figure 4B). We attribute most of this elevation difference to morphology associated with a previously unrecognized lava flow or shallow rhyolite intrusion present but unexposed in lower Pelican Valley (Figure 1A) and extending into Mary Bay, as discussed above. Slightly less than 10 meters of vertical difference in rim height is observed in the seismic profile of the explosion crater between the northern and southern rims. This nearly 10 meter difference may represent doming associated with hydrothermal activity. A currently active example of hydrothermal doming on a much smaller scale can be seen on the southern flank of the large explosion crater (Figure 4B). Here, a seismically opaque area interpreted as a large pocket of gas, probably steam, is present at shallow (<8 meters) depth below the sediment-water interface. Laminated lacustrine sediments show a slight convex-upward doming above this gas pocket that we attribute to uplift. Figure 4B also shows an area on the southern flank where we suggest that a gas pocket breached the surface and is now a hydrothermal vent. Note the attitude of the reflective layers dipping into and draping over the rim of the vent.

Hydrothermal explosions have occurred repeatedly over the past 12 ka in Yellowstone National Park and are primarily confined within the boundaries of the Yellowstone caldera (Figure 1). We interpret the large sublacustrine depressions as post-glacial hydrothermal-explosion craters similar in origin to those on land, such as Duck Lake, Pocket Basin, the 8.3-ka Turbid Lake crater, and the 3.0-ka Indian Pond crater (Figure 3) (Morgan et al. 1998; Muffler et al. 1971; Wold et al. 1977). In

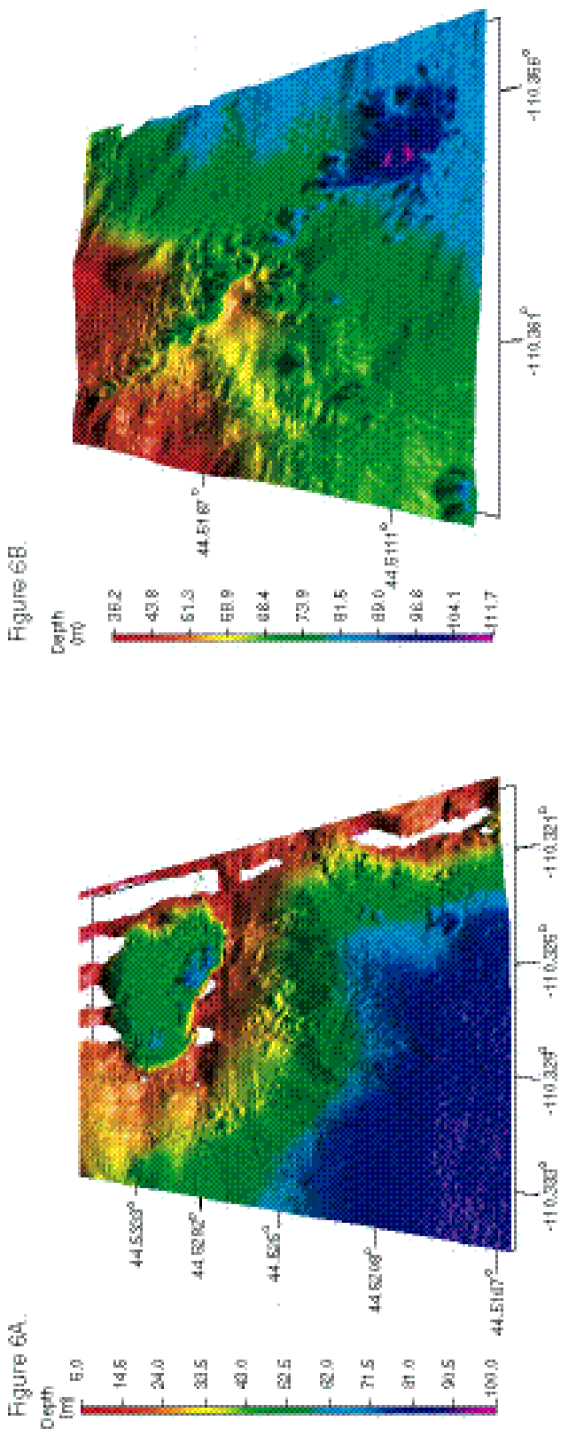

Figure 6. (A) High-resolution bathymetric image of the 800 m Elliott's Crater, an explosion crater in the northern lake. Note deeper, younger internal craters within the large crater and small hydrothermal vent craters on the rim outside the large crater. (B) High-resolution bathymetric image of hydrothermal vent craters along a northwest-trending fissure east of Stevenson Island. The deep hole at the southeastern end of the trend is one of the largest hydrothermal vent areas in the lake and is also the deepest point in the lake at 133 m.

contrast to the subaerial craters, which have radial aprons of explosion breccia ejected during crater formation (Hamilton 1987; Love and Good in press), many of the sublacustrine circular depressions lack an obvious apron. This may indicate either more widespread dispersal of ejection deposits in the lake or that some process, such as collapse associated with hydrothermal alteration, created those depressions.

Small hydrothermal explosion craters on the floor of Yellowstone Lake: Seismic-reflection profiles of the surveyed areas in the northern and West Thumb basins of Yellowstone Lake reveal a lake floor covered with laminated lacustrine muds and diatomite, many of which are deformed, disturbed, and altered. High-resolution bathymetric mapping reveals that many of these areas contain small (<20 m) depressions pockmarking the lake bottom (Figures 3, 6B). In seismic-reflection profiles (Figure 4B), these features typically are imaged as V-shaped structures associated with reflective layers that are deformed or have sediments draped across their edges. Areas of high opacity or no reflection occur directly beneath these features and are interpreted as gas pocket, or hydrothermally altered zones. Evidence for lateral movement of hydrothermal fluids is seen beneath and adjacent to many of these features in seismic-reflection profiles as areas of high opacity or no reflection and in the high-resolution aeromagnetic data as areas of low magnetic intensity which represent a much larger area than seen in the surficial hydrothermal vents (Finn and Morgan 2002). Associated with these vent areas are smaller domal structures in which the laminated diatomaceous lacustrine sediments have been domed upward as much as several meters by underlying pockets of gas, presumably steam.

We interpret these features as sublacustrine hydrothermal vents with associated hydrothermal feeders. We attribute much of the deformation and alteration to hydrothermal vent channelways and subsurface migration of hydrothermal fluids. In contrast, areas devoid of inferred hydrothermal vents show well-laminated seismic reflections characteristic of lake sediments. Over 150 vents have been mapped in the northern lake basin. Several thermal fields also are identified in West Thumb basin including a large northeast-trending thermal-vent field in the southeast, another field in the northwest, and several in the west (Figure 3). These fields contain dozens of small hydrothermal vents.

Siliceous spires: Siliceous spires occur in Bridge Bay (Figure 3) in the northern basin of Yellowstone Lake, discovered in 1997 by Eastern Oceanics and the University of Wisconsin-Milwaukee. Approximately 12–15 spires are identified in water depths of ~15 m. These roughly conical structures (Figure 7A) are up to 8 m in height and up to 10 meters wide at the base. A small 1.4-m-tall spire collected from Bridge Bay in cooperation with the National Park Service on 1999 shows the spire base to be relatively shallow (~0.5 m below the sediment-water interface), irregular, and rounded; spire material above the sediment-water interface constitutes about 75% of the entire structure. The sediment-water interface is recorded on the spire as a zone of banded ferromanganese oxide-stained clay-rich and diatomaceous sediments. Below the sediment-water interface, the spire is non-oxidized. Above the interface, the spire has a dark reddish-brown oxide

coating (Figure 7B). The interior of the collected spire is white, finely porous, and has thin (from 0.3 cm to <3 cm diameter), anastomozing vertical pipe-like structures through which hydrothermal fluids flowed. Little oxide is found in the interior of the spire structure but oxidation surfaces are present on former growth fronts (Figure 7B). Chemical and oxygen-isotope analyses, and scanning electron microscope (SEM) studies of the spires show them to be composed of silicified bacteria, diatom tests, and amorphous siliceous sinter associated with sublacustrine hydrothermal vent processes (Figure 7C). The Bridge Bay spires are strongly enriched in As, Ba, Mn, Mo, Tl, Sb, and W (Figure 7D). Oxygen isotopic ratios suggest formation at about 70–90ºC. U-series disequilibria dating of two samples from one spire both yield a date of about 11 ka (ages were determined by Neil Sturchio, written communication, 1998); thus, the spires are immediately postglacial. Spires may be analogous in formation to black-smoker chimneys, well-documented hydrothermal features associated with deep-seated hydrothermal processes at oceanic plate boundaries (Delaney et al. 2001).

Landslide deposits: Multibeam bathymetric data reveal hummocky lobate terrain at the base of slopes along the northeast and eastern margin of the lake basin (Figure 3). Seismic-reflection data indicate that the deposits range in thickness from 0-10 m at the eastern edge of the lake and become thinner toward the interior of the lake basin. We interpret these as landslide deposits. Proximal deposits at the eastern lake edge are as thick as 10 m near the shore. The distal landslide deposits are much thinner and extend as far as 500 m into the deeper lake basin. The thickness of the lacustrine-sediment cap deposited above the landslide deposits varies and suggests that the landslides were generated by multiple events. We think it is likely that they were triggered by ground shaking associated with earthquakes and (or) hydrothermal explosions. The eastern shore of Yellowstone Lake, near where these landslide deposits occur, marks the margin of the Yellowstone caldera (Christiansen 1984; Christiansen 2001; Hildreth et al. 1984; U.S.G.S. 1972) and abuts steep terrain of the Absaroka Mountains to the east, both possible factors contributing to the landsliding.

Submerged shorelines: Several submerged former lake shorelines form underwater benches in the West Thumb and northern basins of Yellowstone Lake (Figure 3). The submerged, shallow margins (depth <15–20 m) of the northern basin are generally underlain by one to three relatively flat, discontinuous, postglacial terraces that record the history of former lake levels. Correlation of these submerged shoreline terraces around the lake is based primarily on continuity inferred from multibeam bathymetric data and shore-parallel seismic-reflection profiles. These data indicate that lake levels were significantly lower in the past. An extensive bench occurs south of Steamboat Point and along the west shore of the northern basin south of Gull Point. In Bridge Bay, submerged-beach pebbly sand 5.5 m below the present lake level yielded a carbon-14 date of 3,560 ± 60 yr B.P. (Pierce et al. 1997). Well-developed submerged shoreline terraces are present in West Thumb basin, especially along the southern and northern edges.

Relief on these terraces is as much as 2–3 m, a measure of post-depositional vertical deformation. Documentation of the submerged terraces adds to a data-

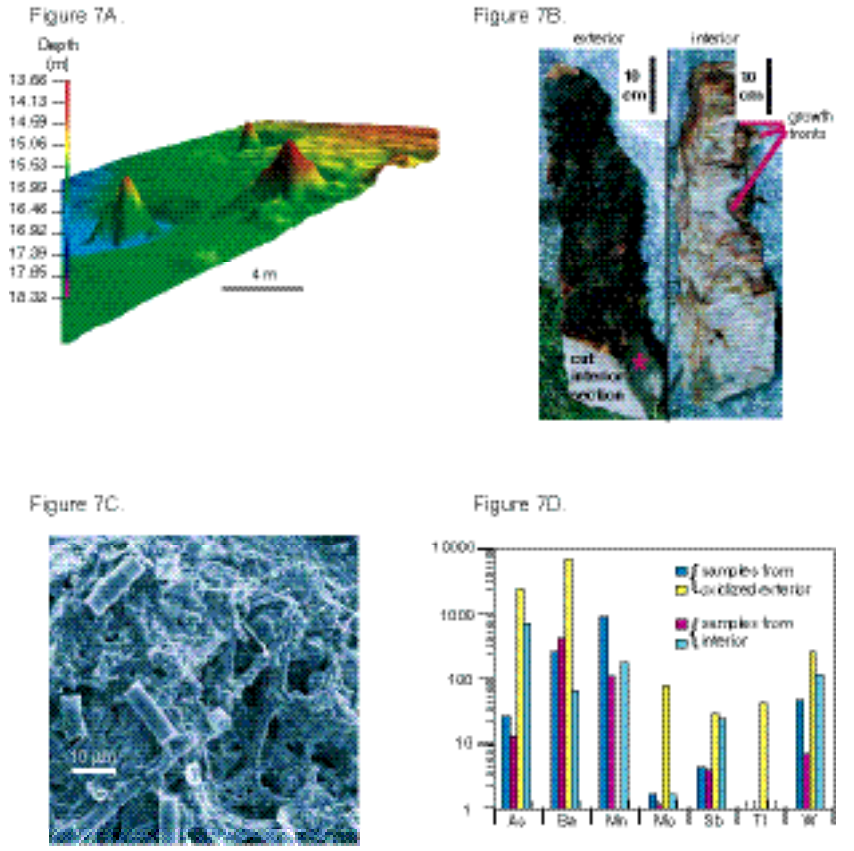

Figure 7. (A) Bathymetric image of spires in Bridge Bay, showing roughly conical shapes. Roughly a dozen such siliceous sinter spires occur near Bridge Bay, some as tall as 8 m. Many of the spires occupy lake-bottom depressions (possible former explosion or collapse craters). (B) Photographs of the exterior and interior of a 1.4 m-tall spire sample recov - ered from Bridge Bay by National Park Service divers. The sediment–water interface of this spire is apparent near the base of the exterior section, as seen in the dramatic change in color in the outer rind of red-brown ferromanganese oxide to the light gray interior. (The red asterisk on the photograph showing the exterior is on a natural external surface of the spire below the sediment–water interface.) Former growth fronts on the spire can be seen as shown in the photograph of the interior section. (C) SEM image of diatoms, silicified filamentous bacteria, and amorphous silica from a spire sample. (D) Summary bar graph of chemical analyses of spire samples showing substantial concentrations of potentially toxic elements: arsenic, barium, manganese, molybdenum, antimony, thallium, and tungsten.

base of as many as 9 emergent terraces around the lake (Locke and Meyer 1994; Locke et al. 1992; Meyer 1986; Pierce et al. 1997). Changes in lake level over the last 9,500 radiocarbon years have occurred primarily in response to episodic uplift and subsidence (inflation and deflation) of the central part of the Yellowstone caldera (Dzurisin et al. 1994; Pelton and Smith 1982; Pierce et al.

1997; Wicks et al. 1998). Holocene changes in lake level recorded by these terraces have been variably attributed to intra-caldera magmatic processes, hydrothermal processes, climate change, regional extension, and (or) glacioisostatic rebound (Dzurisin et al. 1994; Locke and Meyer 1994; Meyer and Locke 1986; Pierce et al. 1997; Wicks et al. 1998).

Fissures and faults: Features identified in the western area of the northern and central basins (Figure 2B) include a set of sub-parallel, elongate, north-northeast-trending fissures west of Stevenson Island extending southward toward Dot Island (Figure 3); a series of en echelon, linear, northwest-trending, fissure-controlled, small depressions east and southeast of Stevenson Island; and a downdropped graben north of Stevenson Island, nearly on strike with Lake Village.

Subparallel fissures west of Stevenson Island (Figure 3) plunge as much as 10-20 m into the soft-sediment lake floor 0.5-km southeast of Sand Point. These fissures represent extension fractures whose orientation is controlled by regional north-south structural trends, recognized both north and south of Yellowstone Lake. Active hydrothermal activity is localized along the fissures as shown by dark oxide precipitates partially coating the surfaces of the fissures and shimmering fluids upwelling from these. The fissures, inspected with the submersible ROV for about 160 meters along their NNE trend are narrow (<2 m wide) and cut vertically into soft laminated sediments with no vertical displacement. A parallel set of N-S-trending fissures also occurs 1.3-km northeast of Sand Point. Farther south along this trend, the fissures appear to have well developed hydrothermal vent craters, although investigations with the submersible show only weak or inactive vent fields in the central basin.

Inspection of the features east of Stevenson Island (Figure 3, 6B) using the submersible ROV indicates that small, well-developed hydrothermal vents coalesce along northwest-trending fissures. These may be similar to but more evolved than those to the west of Stevenson Island. The deepest part of Yellowstone Lake, at 133 m, is in the floor of a hydrothermal vent at the south end of the northernmost set of aligned vents; hydrothermal fluids from vents at this location are as hot as 120°C.

Finally, east-west seismic-reflection profiles across the down-dropped block north of Stevenson Island reveal a north-northwest-trending graben structure bounded by normal faults (Kaplinski 1991; Otis and Smith 1977; Shuey et al. 1977). Measured displacements along the two bounding faults vary, but displacement along the western boundary is generally ~6 m whereas that along the eastern normal fault is ~2 m. The eastern bounding fault cuts Holocene lake sediments indicating recent movement. Seismic profiles across the graben project (or strike) toward Lake Village, posing a potential seismic hazard in that area.

All of the above-described sublacustrine structures, the regional tectonic framework of the northern Rocky Mountains, and the still-active cooling subcaldera magma chamber (Eaton et al. 1975; Fournier 1989; Fournier et al. 1976; Lehman et al. 1982; Stanley et al. 1991; Wicks et al. 1998) play important roles in shaping the morphology of the floor of Yellowstone Lake as revealed in the

bathymetric map, especially of the western part of the northern lake basin. Many of the recently identified features, such as the active fissures west of Stevenson Island and the active graben north of Stevenson Island, are oriented roughly north-south, and may be related to a regional structural feature in western Yellowstone Lake on strike with the Neogene Eagle Bay fault (Figure 1B) (Locke and Meyer 1994; Pierce et al. 1997), perhaps coincident with the inferred margin of the 2.1-Ma Huckleberry Ridge caldera (Christiansen 1984; Christiansen 2001; Hildreth et al. 1984; U.S.G.S. 1972). Seismicity maps of the Yellowstone region (see U.S. Geological Survey Yellowstone Volcano Observatory website: http://volcanoes.usgs.gov/yvo) show concentrations of epicenters along linear N-S trends in the northwestern portion of the lake.

Summary and Conclusions

An important outcome of recent studies in Yellowstone Lake is the extension of the subaerial geologic mapping, allowing the lake basin to be understood in the geologic context of the rest of the Yellowstone region (Blank 1974; Christiansen 1974; Christiansen 2001; Richmond 1973; U.S.G.S. 1972). Rhyolitic lava flows contribute greatly to the geology and morphology of Yellowstone Lake. We infer from our high-resolution bathymetry and aeromagnetic data that Stevenson, Dot, and Frank Islands are underlain by a large-volume rhyolitic lava flows (Figure 3). Mapped late Pleistocene glaciolacustrine sediment deposits on these islands merely mantle or blanket the flows (Otis and Smith 1977; Richmond 1974; Richmond and Waldrop 1975; Shuey et al. 1977). Similarly, the hydrothermally cemented beach deposits exposed on Pelican Roost (Figure 3), located ~1 km southwest of Steamboat Point (Figure 3), may also blanket a submerged large-volume rhyolite flow. The margin of the Yellowstone caldera (Otis and Smith 1977; Richmond 1974; Richmond and Waldrop 1975; Shuey et al. 1977) passes through the central part of the lake and northward along the lake's eastern edge (Figure 1). Similar to most of the rest of the margin of the Yellowstone caldera (Figure 1A), we suggest that postcaldera rhyolitic lava flows are present along much of the caldera margin beneath Yellowstone Lake.

Additional and significant potential hazards inferred from the bathymetric, seismic, and submersible surveys of Yellowstone Lake include the effects of potential hydrothermal explosions and related phenomena, such as the ejection of debris, landsliding along the lake margins, and sudden collapse of the lake floor through fragmentation of hydrothermally altered cap rocks. Any of these events could result in a sudden and dramatic shift in lake level, generating a small tsunami that could cause catastrophic local flooding. Ejecta from past hydrothermal explosions that formed craters in the floor of Yellowstone Lake extend several kilometers from their crater rims and include rock fragments in excess of several meters in diameter (Hamilton 1987; Love and Good in press; Morgan et al. 1998; Richmond 1973; Richmond 1974; Richmond 1976; Richmond 1977). In addition to potential hazards to humans, such explosions are likely to be associated with the rapid release into the lake of steam and hot water (Fournier et al. 1991), possibly affecting water chemistry by the release of potentially toxic trace

metals. Such changes could be significant to the fragile ecosystem of Yellowstone Lake and vicinity (Shanks et al. 2001).

Acknowledgments

We thank Kate Johnson, Ed DuBray, Geoff Plumlee, Pat Leahy, Steve Bohlen, Elliott Spiker, Tom Casadevall, Dick Jachowski, Mike Finley, John Varley, Tom Olliff, and Paul Doss for supporting this work. We thank Dan Reinhart, Lloyd Kortge, Ann Deutch, Jeff Alt, Julie Friedman, Brenda Beitler, Charles Ginsburg, Pam Gemery, Rick Sanzolone, Bree Burdick, Eric White, Jim Bruckner, Jim Waples, Bob Evanoff, Wes Miles, Rick Mossman, Gary Nelson, David Janecke, Tim Morzel, and many others for assistance with field studies. We thank John Berhrendt, Bob Christiansen, Karl Kellogg, and Geoff Plumlee for constructive reviews that substantially improved the manuscript. This research was supported by the Mineral Resources Program, the Climate History Program, the Venture Capital Fund, and the Northern Rocky Mountain Research Center, all of the U.S. Geological Survey, and by the National Park Service and the Yellowstone Foundation.

References

Blank, H.R. 1974. Geologic map of the Frank Island quadrangle, Yellowstone National Park, Wyoming. U.S. Geological Survey, Reston.

Bonnichsen, B., and D.F. Kauffman. 1987. Physical features of rhyolite lava flows in the Snake River plain volcanic province, southwestern Idaho. Pages 119–145 in *The emplacement of silicic domes and lava flows*. J.H. Fink ed., Geological Society of America (GSA), Boulder.

Christiansen, R.L. 1974. Geologic map of the West Thumb Quadrangle, Yellowstone National Park, Wyoming. GQ-1191, U.S. Geological Survey, Reston.

———. 1984. Yellowstone magmatic evolution: Its bearing on understanding large-volume explosive volcanism. Pages 84–95 in *Explosive Volcanism: Inception, Evolution, and Hazards* National Academy Press.

———. 2001. The Quaternary and Pliocene Yellowstone Plateau Volcanic Field of Wyoming, Idaho, and Montana. U.S. Geological Survey Professional Paper 729-G, 145.

Christiansen, R.L., and H.R. Blank, Jr. 1975. Geologic map of the Canyon Village Quadrangle, Yellowstone National Park, Wyoming. GQ-1192, U.S. Geological Survey, Reston.

Delaney, J.R., D.S. Kelley, E.A. Mathez, D.R. Yoerger, J. Baross, M.O. Schrenk, M.K. Tivey, J. Kaye, and V. Robigou. 2001. "Edifice Rex" Sulfide Recovery Project; analysis of submarine hydrothermal, microbial habitat: Eos, *Transactions*, American Geophysical Union, v. 82, no. 6, p. 67, 72–73. et al. 2001.

Dzurisin, D., K.M. Yamashita, and J.W. Kleinman. 1994. Mechanisms of crustal uplift and subsidence at the Yellowstone Caldera, Wyoming. *Bulletin of Volcanology* 56, 261–270.

Eaton, G.P., R.L. Christiansen, H.M. Iyer, A.M. Pitt, D.R. Mabey, H.R. Blank, Jr., I. Zietz, and M.E. Gettings. 1975. Magma Beneath Yellowstone National Park. *Science* 188 (4190), 787–796.

Finn, C.A., and L.A. Morgan. 2002. High-resolution aeromagnetic mapping of volcanic terrain, Yellowstone National Park. *Journal of Volcanology and Geothermal Research*

115, 207–231.

Fournier, R.O. 1989. Geochemistry and dynamics of the Yellowstone National Park hydrothermal system. *Annual Review of Earth and Planetary Sciences* 17, 13–53.

Fournier, R.O, J.M. Thompson, C.G. Cunningham, and R.A. Hutchinson. 1991. Conditions leading to a recent small hydrothermal explosion at Yellowstone National Park. *Geological Society of America Bulletin* 103, 1114–1120.

Fournier, R.O., D.E. White, and A.H. Truesdell. 1976. Convective heat flow in Yellowstone National Park. Pages 731–739 in *Proceedings Second U.N. Symposium on the Development and Use of Geothermal Resources*. U.S. Government Printing Office, Washington D.C., San Francisco.

Hamilton, W.L. 1987. Water level records used to evaluate deformation within the Yellowstone Caldera, Yellowstone National Park. *Journal of Volcanology and Geothermal Research* 31(3–4), 205–215.

Hildreth, W., R.L. Christiansen, and J.R. O'Neil. 1984. Catastrophic isotopic modification of rhyolitic magma at times of caldera subsidence, Yellowstone Plateau volcanic field. *Journal of Geophysical Research* 89(10), 8339–8369.

Kaplinski, M.A. 1991. *Geomorphology and geology of Yellowstone Lake, Yellowstone National Park, Wyoming.* M. Sc. Thesis, Northern Arizona University, Flagstaff, AZ, 82 pp.

Klump, J.V., C.C. Remsen, and J.L. Kaster. 1988. The presence and potential impact of geothermal activity on the chemistry and biology of Yellowstone Lake, Wyoming. Pages 81–98 in *Global Venting, Midwater and Benthic Ecological Processes*. NOAA Symposium on Undersea Research. M. DeLuca and I. Babb eds., NOAA.

Lehman, J.A., R.B. Smith, and M.M. Schilly. 1982. Upper crustal structure of the Yellowstone cladera from seismic delay time analyses and gravity correlations. *Journal of Geophysical Research* 87, 2713–2730.

Locke, W.W., and G.A. Meyer. 1994. A 12,000 year record of vertical deformation across the Yellowstone caldera margin: The shorelines of Yellowstone Lake. *Journal of Geophysical Research* 99, 20,079–20,094.

Locke, W.W., G.A. Meyer, and J.C. Pings. 1992. Morphology of a postglacial fault scarp across the Yellowstone (Wyoming) caldera margin, United States, and its implications. *Bulletin of the Seismological Society of America* 82(1), 511–516.

Love, J.D., J.M. Good, and D. Browne. In press. Lithology, fossils, and tectonic significance of Pleistocene lake deposits in and near ancestral Yellowstone Lake. Shorter Contributions to General Geology, U.S. Geological Survey Professional Paper, Integrated Geoscience Studies in the Greater Yellowstone Area: Volcanic, Tectonic, and Hydrothermal Processes in the Yellowstone Geoecosystem.

Merrill, M.D. 1999. *Yellowstone and the Great West: Journals, Letters, and Images from the 1871 Hayden Expedition.* University of Nebraska Press.

Meyer, G.A. 1986. *Genesis and deformation of Holocene shoreline terraces, Yellowstone Lake, Wyoming*. Master's Thesis.

Meyer, G.A., and W.W. Locke. 1986. Origin and deformation of Holocene shoreline terraces, Yellowstone Lake, Wyoming. *Geology* 14, 699–702.

Morgan, L.A., W.C. Shanks III, D.A. Lovalvo, S.Y. Johnson, W.J. Stephenson, K.L. Pierce, S.S. Harlan, C.A. Finn, G. Lee, M. Webring, B. Schulze, J. Dühn, R. Sweeney, and L. Balistrieri. 2003. Exploration and Discovery in Yellowstone Lake: Results from High-Resolution Sonar Imaging, Seismic Reflection Profiling, and Submersible Studies. *Journal of Volcanology and Geothermal Research* (in press).

Morgan, L.A., W.C. Shanks, K.L. Pierce and R.O. Rye. 1998. Hydrothermal Explosion Deposits in Yellowstone National Park: Links to Hydrothermal Processes. Eos,

Transactions, AGU fall annual meeting 79, F964.

Morgan, P., D.D. Blackwell, R.E. Spafford, and R.B. Smith. 1977. Heat flow measurements in Yellowstone Lake and the thermal structure of the Yellowstone caldera. *Journal of Geophysical Research* 82, 3719–3732.

Muffler, L.J.P., D.E. White, and A.H. Truesdell. 1971. Hydrothermal explosion craters in Yellowstone National Park. *Geological Society of America Bulletin* 82, 723–740.

Otis, R.M., and R.B. Smith. 1977. Geophysical surveys of Yellowstone Lake, Wyoming. *Journal of Geophysical Research* 82, 3705–3717.

Pelton, J.R., and R.B. Smith. 1982. Contermporary vertical surface displacements in Yellowstone National Park. *Journal of Geophysical Research* 87, 2745–2751.

Pierce, K.L. 1974. Surficial geologic map of the Tower Junction quadrangle and part of the Mount Wallace quadrangle, Yellowstone National Park, Wyoming and Montana, U. S. Geological Survey.

———. 1979. History and dynamics of glaciation in the northern Yellowstone National Park area. U.S. Geological Survey Professional Paper 729-F, 89 p.

Pierce, K.L, K.P. Cannon, and G. Meyer. 1997. Yellowstone Caldera "heavy breathing" based on Yellowstone Lake and River changes in post-glacial time. Eos, *Transactions*, American Geophysical Union 78, 802.

Remsen, C.C., J.V. Klump, J.L. Kaster, R. Paddock, P. Anderson, and J.S. Maki. 1990. Hydrothermal springs and gas fumaroles in Yellowstone Lake, Yellowstone National Park, Wyoming. *National Geographic Research*, v. 6, 509–515.

Richmond, G.M. 1973. Surficial geologic map of the West Thumb quadrangle, Yellowstone National Park, Wyoming. U.S.G.S., Reston.

———. 1974. Surficial geologic map of the Frank Island quadrangle, Yellowstone National Park, Wyoming. U.S.G.S., Reston.

———. 1976. Surficial geologic history of the Canyon Village Quadrangle, Yellowstone National Park, Wyoming, for use with map I-652. B 1427, U. S. Geological Survey, Reston.

———. 1977. Surficial geologic map of the Canyon Village Quadrangle, Yellowstone National Park, Wyoming. I-0652, U. S. Geological Survey, Reston.

Richmond, G.M., and H.A. Waldrop. 1975. Surficial geologic map of the Norris Junction quadrangle, Yellowstone National Park, Wyoming.

Shanks, W.C., III, L. Balistrieri, J. Alt, L.A. Morgan, G. Meeker, R.O. Rye, N. Sturchio, D. Lovalvo, R. Cuhel, and J.V. Klump. 2001. Geochemical Studies of Hydrothermal Vents and Sublacustrine Siliceous Deposits in Yellowstone Lake, in Agenda and Abstracts, Yellowstone Lake: Hotbed of Chaos or Reservoir of Resilience? October 8–10, 2001. 6th Biennial Scientific Conference on the Greater Yellowstone Ecosystem, Yellowstone National Park, National Park Service, 35–36.

Shuey, R.T., R.O. Ugland, and R.B. Smith. 1977. Magnetic properties and secular variation in cores from Yellowstone and Jackson Lakes, Wyoming. *Journal of Geophysical Research* 82, 3739–3746.

Smith, R.B. 1991. Earthquake and geodetic surveillance of Yellowstone. Seismological Research Letters. 62, 27.

Stanley, W.D., D.B. Hoover, M.L. Sorey, B.D. Rodriguez and W.D. Heran. 1991. Electrical geophysical investigations in the Norris-Mammoth corridor, Yellowstone National Park, and the adjacent Corwin Springs Known Geothermal Resources Area. *U.S. Geological Survey Water Resources Investigations* 91–4052, D1-D18.

U.S.G.S. 1972. Geologic map of Yellowstone National Park. U.S.G.S., Reston.

Wicks, C.W., Jr., W.R. Thatcher and D. Dzurisin. 1998. Migration of fluids beneath Yellowstone Caldera inferred from satellite radar interferometry. *Science* 282(5388),

458–462.
Wold, R.J., M.A. Mayhew, and R.B. Smith. 1977. Bathymetric and geophysical evidence for a hydrothermal explosion crater in Mary Bay, Yellowstone Lake, Wyoming. *Journal of Geophysical Research* 82(26), 3733–3738.

L. A. Morgan, U.S. Geological Survey, Denver Federal Center, Box 25046, M.S. 966, Denver, Colorado 80225-0046
W. C. Shanks III, U.S. Geological Survey, Denver Federal Center, Box 25046, M.S. 966, Denver, Colorado 80225-0046
David Lovalvo, Eastern Oceanics, Inc., 25 Limekiln Road, West Redding, Connecticut 06856; eoceanics@compuserve.com
M. Webring, U.S. Geological Survey, Denver Federal Center, Box 25046, M.S. 966, Denver, Colorado 80225-0046
G. Lee, U.S. Geological Survey, Denver Federal Center, Box 25046, M.S. 966, Denver, Colorado 80225-0046
W. J. Stephenson, U.S. Geological Survey, Denver Federal Center, Box 25046, M.S. 966, Denver, Colorado 80225-0046
S. Y. Johnson, U.S. Geological Survey, Denver Federal Center, Box 25046, M.S. 966, Denver, Colorado 80225-0046

✧✧✧✧✧